Inhibitory synaptic timescales drive oscillatory regime transitions in recurrent excitatory-inhibitory networks

Siamak Kheiri,[1] Saeed Taghavi,[2] Matjaž Perc,[3,4,5,6,*] and Alireza Valizadeh[1,2,†]

[1]*Physics Department, Institute for Advanced Studies in Basic Sciences (IASBS), Zanjan 45137-66731, Iran*

[2]*Zapata Briceño Institute for Human Intelligence Research, Madrid, Spain*

[3]*Faculty of Natural Sciences and Mathematics, University of Maribor, Koroška cesta 160, 2000 Maribor, Slovenia*

[4]*Community Healthcare Center Dr. Adolf Drolc Maribor, Ulica talcev 9, 2000 Maribor, Slovenia*

[5]*Department of Physics, Kyung Hee University, 26 Kyungheedae-ro, Dongdaemun-gu, Seoul 02447, Republic of Korea*

[6]*University College, Korea University, 145 Anam-ro, Seongbuk-gu, Seoul 02841, Republic of Korea*

(Received 27 February 2026; accepted 11 May 2026; published 5 June 2026)

In recurrent cortical networks, inhibitory kinetics are often assumed to tune oscillation frequency continuously. Using a recurrent excitatory-inhibitory (E-I) model with fixed excitatory synaptic dynamics, we systematically vary inhibitory decay time constants and show instead that inhibitory timescale acts as a control parameter that drives sharp transitions between distinct collective states. The network switches between a coherent high-frequency regime and a coherent gamma-band regime, separated by an intermediate transition state with reduced synchrony and unstable phase coordination. Phase analysis demonstrates that the coherent regimes exhibit distinct, internally consistent E-I coordination patterns, whereas these relationships break down in the transition regime. Dissecting inhibitory pathways reveals that inhibitory-to-inhibitory decay times determine the operative regime, while inhibitory-to-excitatory kinetics primarily adjust oscillation frequency and the width of the transition region without altering the global phase structure. Our results link physiological diversity in inhibitory synaptic timescales to discrete oscillatory regimes in recurrent cortical circuits.

DOI: 10.1103/zmn7-7kf6

I. INTRODUCTION

Cortical and hippocampal networks exhibit rhythmic activity spanning a broad range of frequencies, including gamma-band oscillations (30–80 Hz) and faster high-frequency oscillations (HFOs; >100 Hz) [1–7]. Gamma rhythms are widely observed across cortical and hippocampal areas and have been implicated in sensory processing, attention, and memory-related computations [8–12]. In addition to gamma activity, transient HFOs, including hippocampal ripple events and fast neocortical oscillations, have been reported across species and recording modalities [2,13–16]. The coexistence of gamma and HFO regimes indicates that recurrent excitatory-inhibitory (E-I) networks can support multiple oscillatory modes under distinct dynamical conditions [17–19].

A large body of experimental and theoretical work indicates that inhibitory synaptic interactions play a central role in the generation of gamma-band oscillations [20–25]. In particular, fast-spiking GABAergic interneurons synchronize local neuronal populations through recurrent inhibition, enabling rhythmic activity via interneuron-driven (ING) or pyramidal-interneuron loop (PING) mechanisms [20,22,26,27]. In such networks, the temporal properties of inhibitory postsynaptic currents critically influence the timing of population activity, demonstrating that inhibitory synaptic kinetics act as key determinants of oscillatory frequency and synchrony [21,24,28–30].

Importantly, inhibitory synaptic kinetics in cortex are not uniform. Experimental measurements have shown that the decay time constants of $GABA_A$-mediated inhibitory postsynaptic currents vary substantially across interneuron subtypes, synaptic locations, receptor compositions, and target-cell classes [24,31–33]. Fast perisomatic inhibition, particularly that mediated by parvalbumin-positive fast-spiking interneurons, is characterized by rapid signaling with decay times on the order of a few milliseconds and is well suited to support precise temporal coordination and gamma-frequency synchronization [24,34,35]. In contrast, dendrite-targeting interneurons, distal synaptic contacts, and receptor configurations associated with prolonged GABAergic currents can produce slower inhibitory signals with decay constants extending beyond several milliseconds [32,33]. Moreover, inhibitory microcircuits are organized through distinct pathway motifs: Some interneuron classes preferentially inhibit excitatory principal cells, whereas others preferentially target interneurons and participate in disinhibitory or interneuron-interneuron control loops [36]. Thus, the effective decay times of inhibitory-to-excitatory and inhibitory-to-inhibitory pathways may differ not because individual inhibitory neurons

*Contact author: matjaz.perc@gmail.com

†Contact author: valizadeh@gmail.com

Published by the American Physical Society under the terms of the Creative Commons Attribution 4.0 International license. Further distribution of this work must maintain attribution to the author(s) and the published article's title, journal citation, and DOI.

necessarily express different kinetics at all of their outputs, but because these pathways can be dominated by different interneuron subtypes, synaptic locations, and receptor compositions. Consequently, cortical circuits may simultaneously express fast and slow inhibitory pathways, effectively operating across a continuum of inhibitory timescales.

Previous theoretical and computational studies have demonstrated that inhibitory synaptic decay time strongly influences oscillation frequency in recurrent excitatory-inhibitory networks [21,25,30,37]. In such networks, fast inhibition supports interneuron-driven (ING) rhythms at high frequencies, whereas slower inhibition promotes gamma-band oscillations arising from excitatory-inhibitory loop (PING) interactions [21,26,37]. More recent computational work has further shown that slower inhibitory kinetics relative to excitation facilitate the emergence of coherent gamma oscillations, while faster inhibitory recovery supports higher-frequency oscillatory states [25,30]. Together, these findings suggest that inhibitory synaptic timescale may act not merely as a frequency-tuning factor but as a control parameter governing the collective dynamical state of recurrent networks [38,39].

However, inhibitory interactions are mediated through multiple pathways with distinct functional roles, including inhibitory-to-inhibitory (I $\rightarrow$ I) and inhibitory-to-excitatory (I $\rightarrow$ E) synapses [20,26]. Interneuron-interneuron coupling can generate fast rhythmic activity through mutual inhibition, whereas feedback inhibition onto excitatory neurons participates in slower excitatory-inhibitory loop oscillations [20,22,40]. How the synaptic decay times associated with these distinct inhibitory pathways interact to determine the dominant oscillatory regime of the network remains incompletely understood.

These observations raise a fundamental question: Do inhibitory synaptic timescales continuously tune the frequency of a single underlying oscillatory mechanism, or do they determine which collective coordination regime is expressed by the network? In recurrent excitatory-inhibitory circuits, oscillations may arise through distinct dynamical mechanisms, including interneuron network gamma (ING) and pyramidal-interneuron gamma (PING) interactions, each characterized by different patterns of excitatory-inhibitory population coordination [20,22,26,40,41]. If inhibitory synaptic kinetics act primarily as control parameters over these mechanisms, variation of inhibitory decay times would be expected to induce transitions between dynamically distinct oscillatory states, rather than a gradual modulation of oscillation frequency [38,39,42,43].

Here, we investigate whether inhibitory synaptic decay times act as continuous tuning parameters or as control variables that select between mechanistically distinct oscillatory regimes in recurrent excitatory-inhibitory networks. By systematically varying the decay time constants of inhibitory-to-inhibitory and inhibitory-to-excitatory synapses while holding excitatory dynamics fixed, we demonstrate that inhibitory kinetics organize network activity into discrete dynamical regimes, including coherent high-frequency oscillatory and gamma-band states, separated by an intermediate transition regime characterized by reduced synchrony and unstable phase coordination. These results suggest that the physiological diversity of inhibitory synaptic timescales observed in cortical circuits may enable recurrent networks to operate in qualitatively different dynamical modes, defined by regime-specific patterns of excitatory-inhibitory coordination rather than continuous modulation of a single oscillatory process.

II. METHODS

A. Neurons

Both pyramidal and interneuron cells were modeled as leaky integrate-and-fire neurons [44–46], with potential described by Eq. (1):

$$\tau_m \frac{dV_i(t)}{dt} = -(V_i(t) - V_{\text{rest}}) + \frac{1}{g}\left(\sum_j I_{ij}\right), \tag{1}$$

where V_i represents the membrane potential of the neuron i and $\tau_m = C_m/g$ denotes the membrane time constant, with C_m and g representing the membrane capacitance and conductance, respectively, V_{rest} is the leak (resting) membrane potential, and I_{ij} is the synaptic current from neuron j to neuron i. When a neuron's membrane potential $V_i(t)$ reaches the threshold V_{th}, the neuron emits a spike at time t_i following the absolute refractory period τ_{ref}, after which the membrane potential is reset to V_{reset}. We set the membrane time constant to $\tau_m = 20$ ms for pyramidal cells and $\tau_m = 10$ ms for interneurons. The spike threshold was -52 mV, the resting potential was -70.0 mV, the reset potential was -59.0 mV, and the absolute refractory period was 1 ms. These parameter values follow standard choices in cortical network modeling [21,38,47].

B. Networks

The network comprised $N_I = 60$ interneurons and $N_E = 240$ pyramidal cells, corresponding to a typical cortical excitatory-inhibitory ratio [38,47]. Connections between populations were assigned randomly, as in standard sparse balanced network models [38,47], with a connection probability P_{ij} for any given pair of neurons. Here, the indices i and j denote the presynaptic and postsynaptic neuron types, respectively. Each neuron receives C randomly chosen connections from other neurons in the networks, from which $C_E = P_{ij}N_E$ from excitatory neurons and $C_I = P_{ij}N_I$ from inhibitory neurons, such that $C = C_E + C_I$.

C. Synaptic current

Two types of synaptic currents were implemented, modeling GABAergic (inhibitory) and AMPAergic (excitatory) inputs [21,46]. The synaptic currents were described by Eq. (2):

$$I_{ij} = \bar{g}_{ij} s(t)(E_{\text{rev}} - V_i(t)), \tag{2}$$

where $\bar{g}_{ij}$ denotes the maximum synaptic conductance from presynaptic neuron j to postsynaptic neuron i and E_{rev} is the synaptic reversal potential. The synaptic gating variable $s(t)$ followed a double-exponential time course [21,48]. For each presynaptic spike at time t_j after a delay τ_l, $s(t)$ was updated

TABLE I. Synaptic model parameters.

Excitatory neuron	Inhibitory neuron
$\tau_r = 0.5$ ms	$\tau_r = 0.5$ ms
$\tau_d = 5.0$ ms	$\tau_d = 1$–10 ms (step $= 0.1$ ms)
$E_{ex} = 0$ mV	$E_{in} = -70.0$ mV
$\tau_{\text{delay}} = 2.0$ ms	$\tau_{\text{delay}} = 2.0$ ms
$P_{ee} = 0.4$, $P_{ie} = 0.4$	$P_{ei} = 0.4$, $P_{ii} = 0.4$
$g_{ee} = 0.05$ nS	$g_{ii} = 3.5$ nS
$g_{ie} = 0.6$ nS	$g_{ei} = 0.9$ nS

as

$$s(t) = f(e^{-(t-t_j-\tau_l)/\tau_d} - e^{-(t-t_j-\tau_l)/\tau_r}), \tag{3}$$

where τ_r and τ_d are the rise and decay time constants. The normalization factor f ensures that the peak value of $s(t)$ equals unity, such that the maximum conductance equals $\bar{g}_{ij}$. The conductance peaks at a time

$$t_{\text{peak}} = t_l + \frac{\tau_d \tau_r}{\tau_d - \tau_r} \ln(\tau_d/\tau_r), \tag{4}$$

and the normalization factor follows as

$$f = \frac{1}{e^{-(t_{\text{peak}}-\tau_l)/\tau_d} - e^{-(t_{\text{peak}}-\tau_l)/\tau_r}}. \tag{5}$$

Synaptic kinetics were described by three parameters: the delay τ_l, the rise time constant τ_r, and the decay time constant τ_d. The reversal potential is set to -70 mV for inhibitory synapses and 0 mV for excitatory synapses. The synaptic kinetics and associated parameters are defined as described above, and their values are provided in Table I.

D. External input

External inputs were modeled as AMPA-type synapses, as commonly implemented in balanced cortical network models [38,47], with conductances of 0.2 nS on pyramidal cells and 0.25 nS on interneurons, sharing the same kinetics as recurrent AMPA synapses. These synapses were driven by random Poisson spike trains at a rate of 4 kHz.

E. Numerical methods

All networks were implemented in NEST version 3.8.0 using the `iaf_cond_beta` neuron model [49,50]. Simulations were run with a time step of 0.1 ms for a total duration of $T = 10$ s, where a 200 ms transient initial condition was discarded. Population firing rates were computed separately for excitatory and inhibitory neurons. The population spike train is defined as

$$\rho(t) = \sum_{i=1}^{N} \sum_{k} \delta\left(t - t_i^k\right), \tag{6}$$

where t_i^k denotes the kth spike time of neuron i. The number of spikes in a discrete bin $[t, t + \Delta t)$, with bin width $\Delta t = 1$ ms, is obtained by integrating the spike train,

$$n(t; \Delta t) = \int_t^{t+\Delta t} \rho(\tau)\, d\tau. \tag{7}$$

The population firing rate (Hz per neuron) is then given by normalizing with respect to bin width and population size,

$$r(t; \Delta t) = \frac{n(t; \Delta t)}{N\, \Delta t}. \tag{8}$$

Finally, a smooth firing rate estimate $\tilde{r}(t)$ can be obtained by convolving $r(t; \Delta t)$ with a Gaussian kernel K, of standard deviation 1.0 ms. This narrow smoothing window was chosen to preserve high-frequency oscillatory components, and control analyses confirmed that smoothing did not alter peak frequencies or spectral structure.

$$\tilde{r}(t) = \sum_m K(m)\, r(t - m\Delta t; \Delta t). \tag{9}$$

This procedure was applied over the entire simulation period, excluding the initial 200 ms transient, to yield the full time course of the population firing rate.

The temporal evolution of population activity was analyzed by calculating the power spectral density (PSD) of $\tilde{r}(t)$ using fast Fourier transform-based methods implemented in the Python scientific computing ecosystem. All data processing, statistical analysis, and visualization were performed using the NumPy, SciPy, Pandas, and Matplotlib libraries [51–55]. For each value of the inhibitory synaptic decay time constant (τ_d^{inh}), the PSD was calculated over the post-transient simulation interval. A two-dimensional parameter-frequency PSD map was constructed to display spectral power as a function of oscillation frequency and τ_d^{inh}.

F. Synchrony index

To quantify network synchrony, we computed the spike-train synchrony index based on zero-lag pairwise correlations (PCs) of binned spike trains [38,56]. Spike times of each neuron were binned at a resolution of 1 ms, producing discrete spike-count vectors $r_i[k]$, where i indexes neurons and k indexes time bins. The zero-lag Pearson correlation coefficient between each neuron pair (i, j) was then calculated as

$$\text{PC}_{ij} = \frac{\text{cov}(r_i[k], r_j[k])}{\sigma(r_i[k])\sigma(r_j[k])}, \tag{10}$$

where cov denotes the covariance across bins and σ the standard deviation. By construction, PC_{ij} measures the synchrony at zero time lag. For a population-level measure, we averaged PC_{ij} across all neuron pairs to obtain a single spike-train synchrony index for the network. A synchrony index of 0 indicates uncorrelated firing, while 1 indicates perfect synchrony.

G. Spike-train synchrony: SPIKE-distance

To address the bin-size dependence of the pairwise correlation measure, we additionally quantified network synchrony using the SPIKE-distance [57–59], a parameter-free, time-resolved measure of spike-train dissimilarity. Unlike correlation-based approaches, the SPIKE-distance operates directly on spike times without requiring binning, making it sensitive to the precise timing of spikes rather than rate fluctuations. For each pair of spike trains (m, n), the SPIKE-distance computes an instantaneous dissimilarity profile $S_{mn}(t)$ based on the relative timing of the nearest spikes

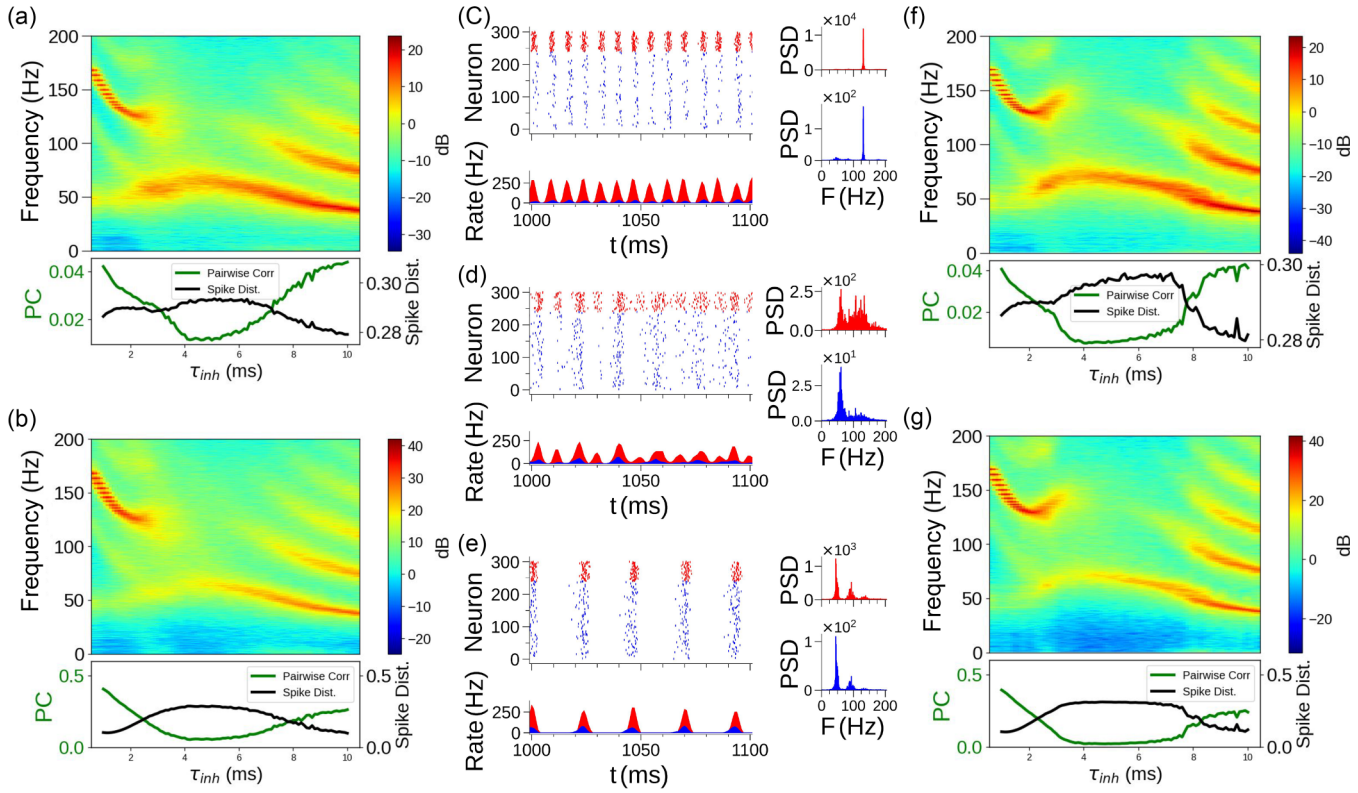


FIG. 1. Network dynamics and spectral properties as function of the inhibitory synaptic decay time constant. PSD of the neuronal populations as a function of frequency and inhibitory synaptic decay time constant, with $\tau_{\text{exc}} = 5$ ms. (a) Excitatory population. (b) Inhibitory population. The color scale represents PSD amplitude in decibels (dB). The bottom panels show the synchrony index vs τ_{inh}, quantified by both the pairwise correlation (green line) and the SPIKE-distance D_S^a (black line). For short decay times ($\tau_{\text{inh}} \lesssim 3$ ms), the network exhibits high-frequency oscillations (>100 Hz) with elevated synchrony. At intermediate values ($\tau_{\text{inh}} \approx 3$–5 ms), excitatory-inhibitory loop competition produces weaker oscillations spanning both the gamma and HFO ranges, accompanied by reduced synchrony. For longer decay times ($\tau_{\text{inh}} \gtrsim 5$ ms), gamma-band oscillations (30–80 Hz) dominate, while HFOs are suppressed. (c)–(e) Population rastergrams (left) and corresponding power spectra (right). The bottom panels show the population firing rates as a function of time (blue: excitatory; red: inhibitory). Top panel: $\tau_{\text{inh}} = 2.0$, ms. Middle panel: $\tau_{\text{inh}} = 3.5$, ms. Bottom panel: $\tau_{\text{inh}} = 8.0$, ms. (f), (g) Same as panels (a) and (b), but for a larger network of $N = 1000$ neurons, confirming that the spectral properties and synchrony results are robust to network size.

in each train. A value of $S_{mn}(t) = 0$ indicates perfect synchrony at time t, while larger values reflect greater temporal mismatch. For a population-level measure, the instantaneous pairwise profiles were averaged over all neuron pairs at each time point, and then averaged over the analysis window:

$$D_S^a = \frac{1}{T}\int_0^T \frac{1}{N(N-1)/2}\sum_{n=1}^{N-1}\sum_{m=n+1}^{N} S_{mn}(t)dt, \qquad (11)$$

where N is the number of neurons and T is the duration of the analysis window. D_S^a is bounded in [0, 1], where 0 indicates perfect synchrony and larger values indicate greater temporal dissimilarity across the population. All computations were performed using the PySpike library [60]. The resulting D_S^a as a function of the inhibitory synaptic time constant τ_{inh} is shown alongside the pairwise correlation index in the bottom panels of Fig. 1 for both the excitatory and inhibitory populations, and for network sizes of $N = 300$ [panels (a) and (b)] and $N = 1000$ [panels (f) and (g)].

H. Phase analysis of excitatory-inhibitory population activity

To quantify the phase relationship between excitatory (E) and inhibitory (I) population activities, population firing-rate time series (prior to Gaussian smoothing) were mean centered to remove the DC component. Signals were then bandpass filtered using a fifth-order Butterworth filter implemented in second-order sections and applied in a zero-phase manner (forward-backward filtering) to avoid phase distortion. For canonical frequency-band analysis, signals were filtered separately in the Gamma (30–80 Hz) and high-frequency oscillation (100–200 Hz) bands.

The analytic signal and instantaneous phase associated with a filtered signal $x(t)$ were defined as

$$z(t) = x(t) + i\,\mathcal{H}\{x(t)\}, \qquad (12)$$

$$\phi(t) = \arg\left(z(t)\right), \qquad (13)$$

where $\mathcal{H}$ denotes the Hilbert transform. Using the instantaneous phases of the excitatory and inhibitory population activities, the phase difference was computed as

$$\Delta\phi(t) = \arg(e^{i(\phi_E(t)-\phi_I(t))}), \qquad (14)$$

ensuring proper circular wrapping in the interval.

To assess phase coordination at the network's dominant oscillatory mode, signals were bandpass filtered around the peak frequency identified from the power spectrum (±10 Hz). The instantaneous E-I phase difference was then computed as above, used as a time-resolved measure of phase locking, and its mean was calculated via the circular average.

III. RESULTS

A. Inhibitory synaptic timescale controls oscillatory regimes

We investigated how the inhibitory synaptic decay time constant shapes collective oscillatory activity in a recurrent excitatory-inhibitory network. Systematic variation of the inhibitory decay time revealed a sharp reorganization of network dynamics, giving rise to distinct oscillatory regimes (Fig. 1).

For short inhibitory decay times ($\tau_{\text{inh}} \ll \tau_{\text{exc}} = 5$ ms), the network exhibited coherent high-frequency oscillations (>100 Hz), reflecting fast inhibitory recovery and interneuron-dominated rhythmicity [Figs. 1(a)–1(c)]. As the inhibitory decay time constant increased, the dominant oscillatory frequency progressively decreased, and an intermediate dynamical regime emerged in which oscillatory activity was distributed across a broader frequency range. Rather than being fully suppressed, rhythmic activity in this regime reflected the coexistence of multiple oscillatory components, resulting in a widened spectral profile accompanied by reduced synchrony at the population level [Fig. 1(d)].

In this range of inhibitory timescales, the fast inhibitory-driven rhythm and the slower excitatory-inhibitory feedback loop both contribute to network dynamics, preventing the emergence of a single dominant oscillatory mode. As a consequence, population activity exhibits weaker coherence [Figs. 1(a) and 1(b), lower panels] and increased temporal variability [see Fig. 1(d)] compared to either the HFO or gamma-band regimes. We have used two different synchrony measures: the mean pairwise correlation of binned spike trains and the SPIKE-distance, a binning-independent measure of spike-time alignment (see Sec. II). Both metrics consistently identify this regime as a state of reduced coordination. In particular, while the correlation decreases, the SPIKE-distance increases (with larger values indicating less precise spike-time alignment), confirming a reduction in synchrony. Although the absolute values differ across populations, reflecting differences in firing statistics, the qualitative reduction in synchrony in the transition regime is robust across metrics.

For sufficiently long inhibitory decay times ($\tau_{\text{inh}} > \tau_{\text{exc}}$), the network settled into a coherent gamma-band oscillation (30–80 Hz) robustly expressed by both excitatory and inhibitory populations [Fig. 1(e)]. Notably, the emergence and stabilization of gamma-band oscillations for $\tau_{\text{inh}} > \tau_{\text{exc}}$ is consistent with recent findings [30], which demonstrate that slower inhibitory kinetics relative to excitation favor coherent gamma rhythms in recurrent excitatory-inhibitory circuits.

Network activity and spectral analysis indicate that the transition between the HFO and gamma regimes does not reflect a gradual slowing of a single oscillatory mode with increasing τ_{inh}. Instead, these rhythms correspond to distinct dynamical states of the network, separated by a transition range of inhibitory decay times in which fast and slow frequency components coexist.

To assess the robustness of these findings, we repeated the analysis for a larger network of $N = 1000$ neurons [Figs. 1(f) and 1(g)]. The spectral organization and synchrony profiles remained qualitatively consistent across network sizes, confirming that the observed oscillatory regimes are not a finite-size artifact. Furthermore, network synchrony was independently quantified using the SPIKE-distance D_S^a, a parameter-free timing-based measure, alongside the pairwise correlation index. As expected from their definitions, the two measures exhibit an inverse relationship: the pairwise correlation index increases with synchrony, while D_S^a increases with dissimilarity. Despite this difference in convention, both measures are in close agreement across all conditions [Figs. 1(a), 1(b), 1(f), and 1(g), bottom panels], confirming that the synchrony results are robust and independent of the binning parameters inherent to the pairwise correlation approach.

B. Differential effects of inhibitory pathways on oscillatory dynamics

To disentangle the relative contributions of distinct inhibitory pathways to the emergence of network oscillatory regimes, we systematically varied the inhibitory-to-inhibitory ($\tau^{\text{inh}}_{I\to I}$) and inhibitory-to-excitatory ($\tau^{\text{inh}}_{I\to E}$) synaptic decay times while keeping other parameters fixed. This analysis revealed a clear hierarchy between inhibitory pathways in determining the global dynamical state of the network.

When the inhibitory-to-excitatory decay time constant was short and $\tau^{\text{inh}}_{I\to I}$ was varied [Figs. 2(a) and 2(d)], the network consistently exhibited three distinct dynamical regimes: a high-frequency oscillatory state at short inhibitory-to-inhibitory decay times, a transition range characterized by the coexistence of fast and slow oscillatory components, and a coherent gamma-band oscillatory state at longer inhibitory-to-inhibitory decay times. Notably, population coherence was substantially higher within the inhibitory subnetwork than in the excitatory population, as reflected by the different dynamic ranges in their respective spectral representations and network coherence [Fig. 2(a)], indicating that collective rhythmic activity is primarily organized by inhibitory interactions even when excitatory neurons remain weakly synchronized.

It is important to note that synchrony estimates based on pairwise correlation can underestimate coordination in regimes where neuronal firing is sparse. In particular, in the high-frequency oscillatory regime, excitatory neurons exhibit low firing rates despite participating in a coherent population rhythm. As a result, many neuron pairs do not fire within the same time bins, leading to reduced pairwise correlations even when population-level synchrony is preserved. This effect is reflected in the weaker synchrony signature of the excitatory population compared to the inhibitory population and compared the two other regimes over which the excitatory neurons fire less sparsely [Figs. 2(a) and 2(b)].

Increasing the inhibitory-to-excitatory decay time constant progressively reduced the mean firing rate of the excitatory population [Figs. 2(b), 2(c), 2(e), and 2(f)], reflecting enhanced temporal integration of inhibitory input onto

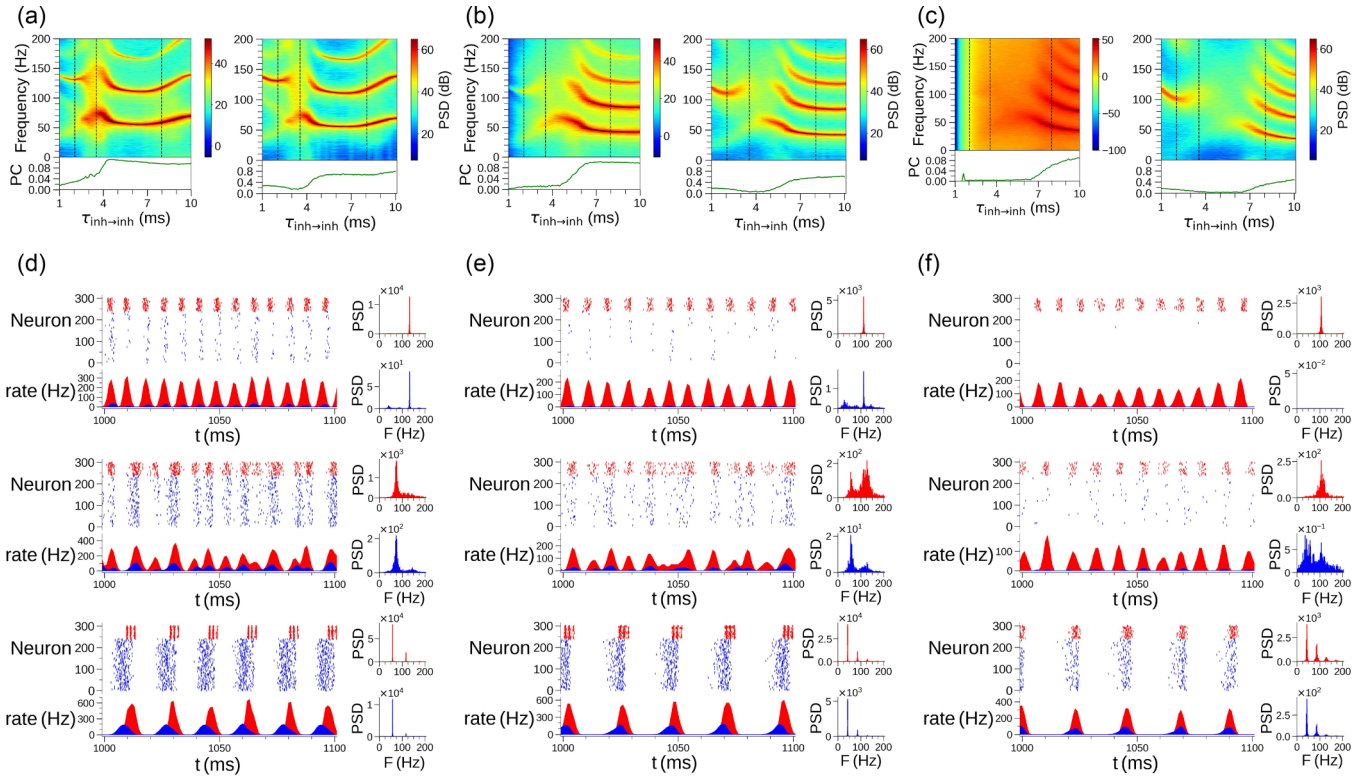


FIG. 2. Network dynamics when the synaptic decay time constant of the inhibitory-to-excitatory connection is held constant at 2.0, 4.0, and 7.0 ms, while the inhibitory-to-inhibitory synaptic decay time constant is varied. parameter-dependent PSD maps are shown, with oscillation frequency on the y axis and inhibitory-to-inhibitory synaptic decay time constant on the x axis; color indicates spectral power. (a)–(c) Excitatory population (left) and inhibitory population (right) for $\tau_{\text{inh}\to\text{exc}} = 2.0$, 4.0, and 7.0 ms, respectively. (d)–(f) Rastergrams (top) and the population firing rate $\langle r(\tilde{t})\rangle$ as a function of time (bottom) for $\tau_{\text{inh}\to\text{inh}} = 1.5$ ms (top), 3.5 ms (middle), and 8.0 ms (bottom), corresponding to panels (a)–(c), respectively.

excitatory neurons. This reduction weakened the expression of HFO activity in the excitatory population at short $\tau^{\text{inh}}_{I\to I}$. Nevertheless, its residual activity continued to exhibit fast temporal modulation imposed by the high-frequency oscillations generated within the inhibitory subnetwork. On the other hand, all three dynamical regimes remained clearly observable in the inhibitory subnetwork, whose activity continued to exhibit robust oscillatory structure across the full range of $\tau^{\text{inh}}_{I\to E}$ considered [Figs. 2(a)–2(c)].

Across different values of the inhibitory-to-excitatory decay time, the gamma-band oscillations that emerged at larger inhibitory-to-inhibitory decay times were comparatively insensitive to changes in inhibitory-to-excitatory decay, indicating that gamma frequency is set predominantly by inhibitory-to-inhibitory timescales once this regime is established [Figs. 2(a)–2(c)]. An additional effect of increasing the inhibitory-to-excitatory decay time was a widening of the transition region between the HFO and gamma regimes. For larger inhibitory-to-excitatory decay times, the range of inhibitory-to-inhibitory decay values over which oscillatory activity was weak and poorly synchronized expanded, and the onset of coherent gamma oscillations was shifted to larger inhibitory-to-inhibitory decay times [Figs. 2(a)–2(c)]. This suggests that while inhibitory-to-excitatory kinetics do not determine the existence of the oscillatory phases, they modulate the sharpness and location of the transition between them.

These observations are consistent with the complementary analysis shown in Fig. 3, in which the inhibitory-to-inhibitory decay time was held fixed while the inhibitory-to-excitatory decay time was varied. In this case, the identity of the dominant oscillatory regime was entirely determined by the fixed inhibitory-to-inhibitory decay time: for short values, the network expressed high-frequency oscillations across the full range of inhibitory-to-excitatory decay values [Figs. 3(a) and 3(d)], and for long values, gamma-band oscillations were expressed throughout [Figs. 3(c) and 3(f)]. In both cases, however, increasing the inhibitory-to-excitatory decay time progressively reduced population synchrony, without triggering a switch to a different oscillatory regime. This effect was most apparent in the gamma regime, where sufficiently large inhibitory-to-excitatory decay times led to a near-complete loss of coherent oscillatory activity [Fig. 3(c)], while the identity of the regime—as opposed to its coherence—remained intact. For intermediate inhibitory-to-inhibitory decay times, the network resided in the transition low-synchrony regime across most of the inhibitory-to-excitatory range [Figs. 3(b) and 3(e)]. Critically, in none of these cases did varying the inhibitory-to-excitatory decay time alone trigger a switch between the high-frequency and gamma regimes. Instead, increasing inhibitory-to-excitatory decay times progressively reduced population synchrony within whichever regime was set by the inhibitory-to-inhibitory timescale, and widened the

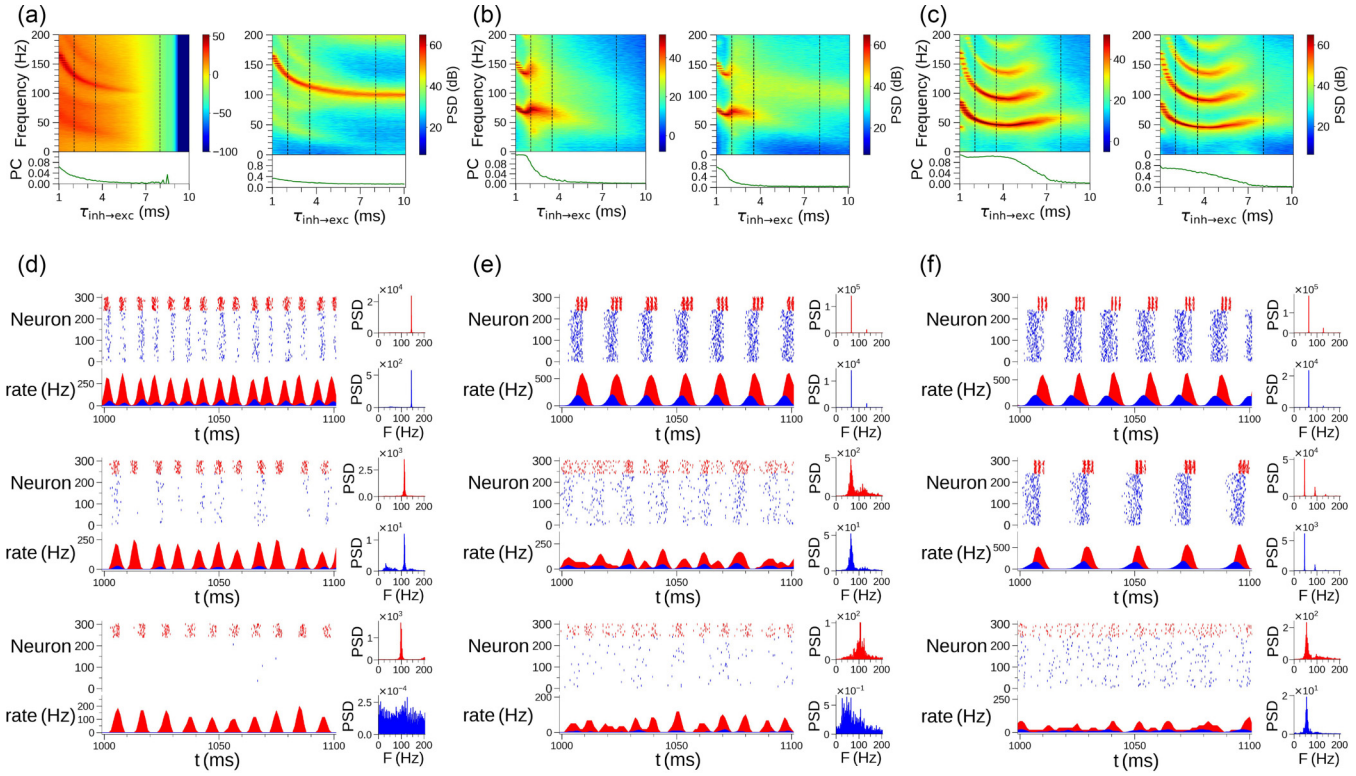


FIG. 3. Network dynamics when the synaptic decay time constant of the inhibitory-to-inhibitory connection is held constant at 2.0, 4.0, and 7.0 ms, while the inhibitory-to-excitatory synaptic decay time constant is varied. Parameter-dependent PSD maps are shown, with oscillation frequency on the y axis and inhibitory-to-excitatory synaptic decay time constant on the x axis; color indicates spectral power. (a)–(c) Excitatory population (left) and inhibitory population (right) for $\tau_{\text{inh}\to\text{inh}} = 2.0$, 4.0, and 7.0 ms, respectively. (d)–(f) Rastergrams (top) and the population firing rate $\langle r(\tilde{t})\rangle$ as a function of time (bottom) for $\tau_{\text{inh}\to\text{exc}} = 1.5$ ms (top), 3.5 ms (middle), and 8.0 ms (bottom), corresponding to panels (a)–(c), respectively.

transition region, without altering the fundamental regime identity.

Taken together, Figs. 2 and 3 demonstrate a clear hierarchy between the two inhibitory pathways. Inhibitory-to-inhibitory synaptic kinetics determine the global oscillatory regime of the network, selecting between the high-frequency, transition, and gamma-band states. Inhibitory-to-excitatory synaptic kinetics, in contrast, do not switch the network between these regimes; rather, they modulate synchrony levels, oscillation frequencies, and the width of the transition region within the regime structure imposed by inhibitory-to-inhibitory interactions. This distinction between regime identity on one hand and synchrony modulation on the other reflects a functional division of labor between the two inhibitory pathways, in which interneuron-to-interneuron kinetics set the operative dynamical state and inhibitory feedback onto excitatory neurons shapes the coherence and frequency of the resulting rhythm.

This hierarchical control is consistent with an interpretation in which inhibitory-to-inhibitory interactions set the dominant interneuron-driven timescale of the network and thereby determine the global oscillatory phase, while inhibitory-to-excitatory interactions primarily modulate oscillation frequency and coherence, most visibly in the high-frequency regime. The mixed dependence of high-frequency oscillations on both inhibitory pathways suggests that interneuron-driven and excitatory-inhibitory loop mechanisms may coexist and jointly shape network rhythms, making a strict separation between ING- and PING-dominated dynamics difficult to infer from population-level activity alone [26,40].

C. State-space organization of oscillatory dynamics

The combined effects of inhibitory-to-inhibitory and inhibitory-to-excitatory synaptic decay times on network oscillations are summarized in Fig. 4, which presents a two-dimensional phase-space representation of peak oscillation frequency and spectral power across the parameter space defined by these decay constants. For each point in this space, oscillatory properties were quantified separately for excitatory (upper panels) and inhibitory (lower panels) populations, allowing direct comparison of their respective contributions to the emergent rhythm.

Across the parameter space, excitatory and inhibitory populations exhibit nearly identical peak oscillation frequencies within both the HFO and gamma bands [Figs. 4(a) and 4(c)], indicating that the network operates at a shared oscillatory timescale regardless of population identity. However, this apparent symmetry in frequency is accompanied by a pronounced asymmetry in oscillatory power [Figs. 4(b) and 4(d)]. Inhibitory neurons consistently display higher peak spectral power than excitatory neurons within the same frequency

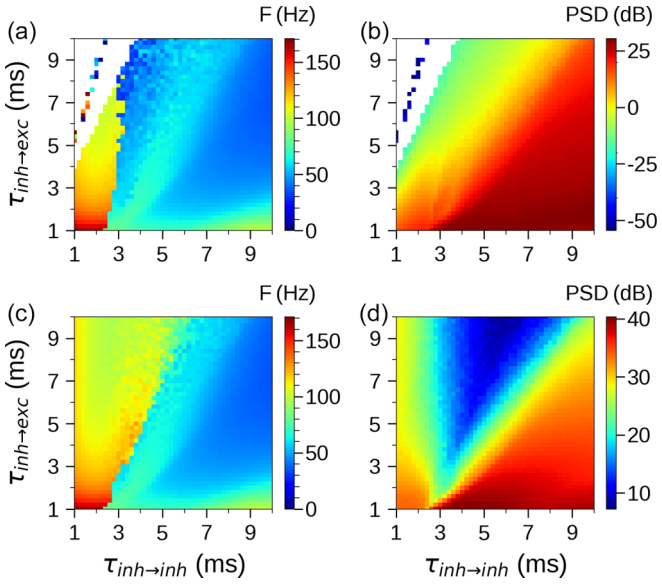


FIG. 4. Peak oscillation frequency and corresponding spectral power as a function of inhibitory synaptic decay time constants. Panel (a) (top left) shows the peak oscillation frequency (Hz) of the excitatory population, and panel (b) (top right) shows the corresponding peak spectral power (dB). Panel (c) (bottom left) shows the peak oscillation frequency of the inhibitory population, and panel (d) (bottom right) shows the corresponding peak spectral power. Peak values were extracted from the population power spectral density in the 0–200 Hz range. In all panels, the horizontal axis represents the inhibitory-to-inhibitory decay time constant $\tau_{\mathrm{inh}\to\mathrm{inh}}$ (ms) and the vertical axis represents the inhibitory-to-excitatory decay time constant $\tau_{\mathrm{inh}\to\mathrm{exc}}$ (ms). The grid resolution for both parameters is 0.2 ms. A distinct low-power region [panel (d)] corresponds to weak spectral peaks, indicating reduced population coherence consistent with the transition state. For fixed $\tau_{\mathrm{inh}\to\mathrm{inh}}$, increasing $\tau_{\mathrm{inh}\to\mathrm{exc}}$ produces a progressive decrease in both peak frequency and peak power [panels (a)–(d)], suggesting that slower inhibition onto excitatory neurons weakens rhythmic synchronization and expands the irregular activity regime. In contrast, for fixed $\tau_{\mathrm{inh}\to\mathrm{exc}}$, increasing $\tau_{\mathrm{inh}\to\mathrm{inh}}$ induces a structured shift in the dominant oscillatory frequency [panels (a) and (c)]: short $\tau_{\mathrm{inh}\to\mathrm{inh}}$ supports high-frequency oscillations, intermediate values yield a transition regime characterized by weak synchrony, and longer $\tau_{\mathrm{inh}\to\mathrm{inh}}$ stabilize oscillations within the gamma band. Notably, peak power increases in the gamma regime [panels (b) and (d)], indicating enhanced population synchrony and underscoring the critical role of recurrent inhibitory timescales in shaping both oscillation frequency and coherence.

band, reflecting a substantially greater degree of population-level synchrony.

This dissociation between common oscillation frequency and differential synchrony suggests that both populations participate in the same global oscillatory mode, but that the rhythm is in general organized within the inhibitory subnetwork. In this regime, excitatory neurons appear to be entrained to an oscillatory timescale primarily determined by interneuron interactions rather than jointly determining the period of the network rhythm. Consistent with this interpretation, short inhibitory-to-inhibitory decay times robustly support coherent high-frequency oscillations across a broad range of inhibitory-to-excitatory values, whereas long inhibitory-to-inhibitory decay times give rise to coherent gamma-band activity with similarly elevated inhibitory synchrony.

Within this phase structure, inhibitory-to-excitatory synaptic decay plays a secondary but non-negligible role. Changes along the inhibitory-to-excitatory axis modulate oscillatory power and frequency without altering the dominant regime. Increasing inhibitory feedback onto excitatory neurons tends to reduce spectral power and broaden the low-coherence transition region separating HFO and gamma states [Figs. 4(b) and 4(d)], suggesting that inhibitory-to-excitatory kinetics primarily regulate the strength and frequency of rhythmic entrainment rather than acting as a control parameter to determine the dynamical regime of the oscillation itself.

Taken together, these phase-space maps indicate that inhibitory-to-inhibitory synaptic kinetics define the operative oscillatory regime of the network, while inhibitory-to-excitatory interactions tune the degree to which excitatory activity is recruited into the inhibition-paced rhythm. The resulting organization reflects a shared frequency structure with population-specific synchrony, consistent with a dominant inhibitory contribution to rhythm generation across oscillatory regimes.

D. Mechanistic origins of oscillatory regimes: Population phase coordination

Figure 5 illustrates how inhibitory synaptic timescales shape the temporal coordination between excitatory and inhibitory population activities across representative decay times corresponding to the HFO, transition, and gamma regimes. Phase analysis of the population firing rates, computed as described in Sec. II, reveals regime-specific patterns of E-I coordination.

At short inhibitory decay times ($\tau_{\mathrm{inh}} = 2$ ms), the network exhibits coherent high-frequency oscillations. In this regime, inhibitory population activity systematically precedes excitatory firing within each oscillatory cycle [Figs. 5(a) and 5(b)], indicating that interneuron dynamics set the pacing of the population rhythm. This temporal ordering is inconsistent with a PING-like mechanism, which requires excitation to recruit inhibition, and instead suggests that excitatory neurons are entrained to an oscillatory timescale determined by interneuron interactions.

For long inhibitory decay times ($\tau_{\mathrm{inh}} = 8$ ms), the network settles into a coherent gamma-band oscillatory state [Figs. 5(e) and 5(f)]. Notably, the phase relationship between excitatory and inhibitory populations remains well defined within this regime, but differs from that observed in the HFO state. In contrast, at intermediate inhibitory decay times ($\tau_{\mathrm{inh}} = 4$ ms), corresponding to the transition regime, population phase coordination breaks down [Figs. 5(C) and 5(D)]. The instantaneous phase difference between E and I activities exhibits large temporal fluctuations and broadened distributions in both the HFO and gamma bands, indicating intermittent or unstable phase locking.

Importantly, within both the HFO and gamma regimes, the phase relations between excitatory and inhibitory populations remain internally consistent, whereas these relations become highly variable in the transition region. This suggests that

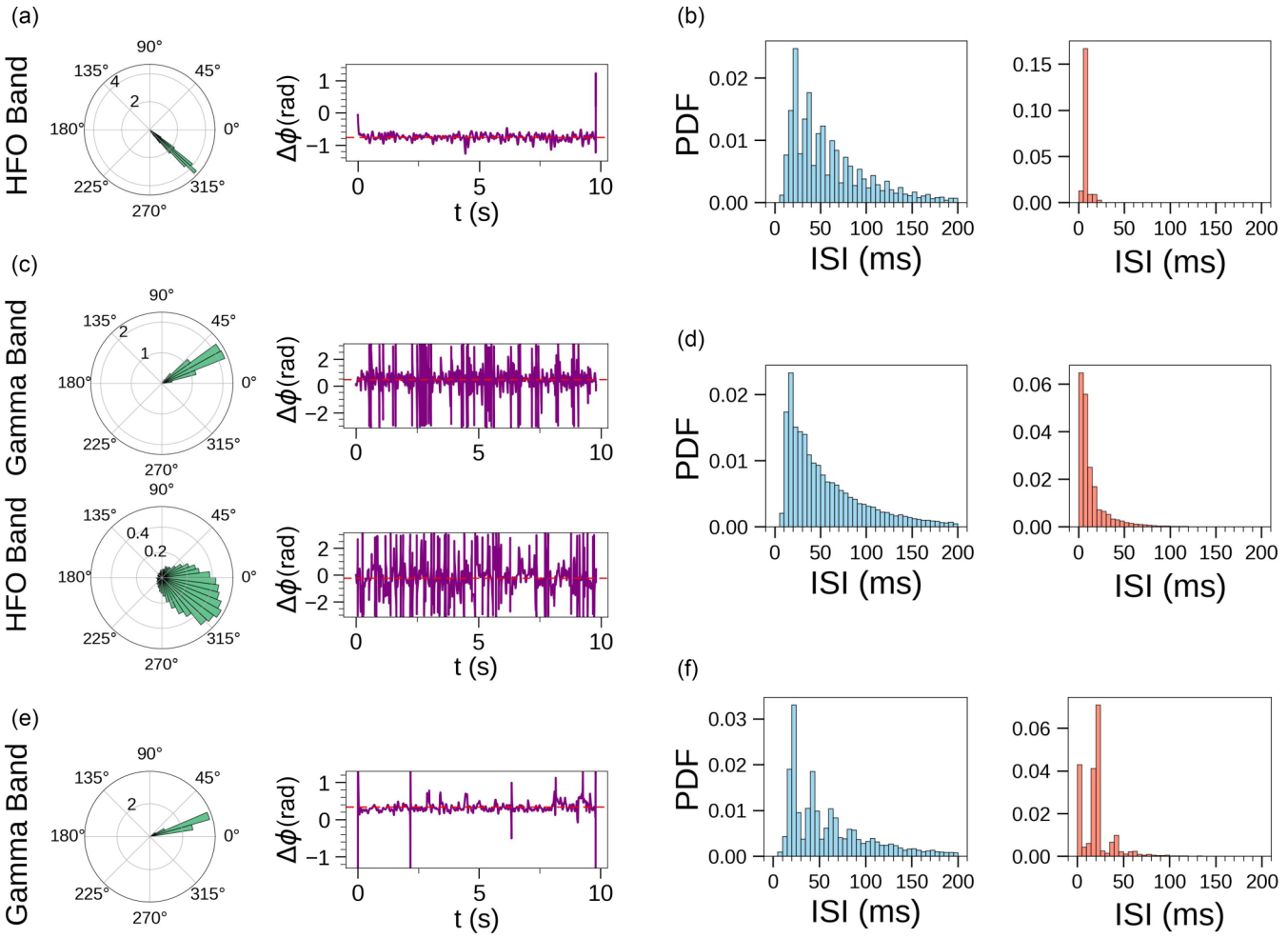


FIG. 5. Network dynamics, E-I phase relationship, and spike-train statistics for different inhibitory synaptic decay time constants. (a), (b) $\tau_{\text{inh}} = 2$ ms; (c), (d) $\tau_{\text{inh}} = 4$ ms; (e), (f) $\tau_{\text{inh}} = 8$ ms. (a), (c), and (d) excitatory-inhibitory phase relationship. Left panel: Polar histograms of the instantaneous phase difference $\Delta\phi(t) = \phi_E(t) - \phi_I(t)$ computed in the Gamma and HFO bands. Right panels: Time-resolved instantaneous E-I phase difference computed around the dominant spectral peak. (b), (d), and (f) Interspike interval (ISI) distributions, excitatory (blue) and inhibitory (red) populations.

the HFO and gamma states correspond to distinct dynamical regimes characterized by stable but different patterns of E-I coordination, rather than representing a continuous modulation of a single oscillatory mechanism. The transition regime thus reflects a loss of coherent regime-specific coordination, appearing consistent with dynamical competition between oscillatory modes.

Taken together, these results indicate that inhibitory synaptic timescale not only tunes oscillation frequency but also controls the organization of excitatory-inhibitory population dynamics, shifting the network between mechanistically distinct oscillatory regimes defined by their characteristic phase coordination.

IV. DISCUSSION

Oscillatory activity in the gamma (30–80 Hz) and high-frequency (>100 Hz) bands is widely observed across cortical and hippocampal circuits and has been implicated in a variety of cognitive and computational functions, including sensory integration, memory encoding, and attentional selection [1,3,11]. In particular, transient high-frequency oscillations, including ripple-like activity, have been reported in both hippocampal and neocortical networks during periods of coordinated population activity, suggesting that recurrent excitatory-inhibitory interactions support multiple coexisting oscillatory modes within local circuits [2,61].

Such oscillations are thought to play a central role in regulating signal transmission and effective connectivity in the brain [62–65]. Rhythmic synchronization of neuronal populations has been proposed to facilitate communication between distributed cortical areas by temporally aligning windows of excitability, thereby enhancing synaptic efficacy and selective information routing [11,12]. Within this framework, the coordination of excitatory and inhibitory population dynamics determines not only the strength but also the temporal precision of interareal interactions, linking local circuit mechanisms to large-scale functional connectivity. Such oscillations are thought to play a central role in regulating signal transmission and effective connectivity in the brain. Rhythmic synchronization of neuronal populations has been proposed to facilitate communication between distributed

cortical areas by temporally aligning windows of excitability, thereby enhancing synaptic efficacy and selective information routing [11,12]. Within this framework, the coordination of excitatory and inhibitory population dynamics determines not only the strength but also the temporal precision of interareal interactions, linking local circuit mechanisms to large-scale functional connectivity [66].

Importantly, inhibitory synaptic kinetics in cortical circuits are not uniform. Experimental studies have demonstrated that the decay time constants of $GABA_A$-mediated inhibitory postsynaptic currents vary substantially across interneuron subtypes and synaptic targets. Synapses formed by fast-spiking parvalbumin-positive interneurons can exhibit rapid decay kinetics on the order of 1–3 ms, whereas dendrite-targeting interneurons may produce considerably slower inhibitory currents [23,24,31]. This physiological diversity implies that cortical microcircuits may simultaneously express inhibitory pathways operating across a continuum of timescales, including very fast synaptic interactions capable of supporting rapid population dynamics.

Previous theoretical and experimental work has identified multiple candidate mechanisms underlying rhythmic activity in recurrent E-I networks, most prominently ING and PING dynamics [20,21,26,38]. In ING-type rhythms, oscillatory activity emerges primarily from mutual inhibition among interneurons, whereas PING dynamics rely on feedback loops in which excitation recruits inhibition to terminate each oscillatory cycle [25,26,30]. Although these mechanisms are often treated as distinct, recent work has suggested that cortical rhythms may instead reflect mixed or regime-dependent interactions between excitatory and inhibitory populations.

In this work, we show that inhibitory synaptic decay time acts as a control parameter that organizes recurrent E-I networks into dynamically distinct oscillatory regimes. Phase-space analysis reveals that inhibitory-to-inhibitory synaptic kinetics determine the dominant oscillatory regime expressed by the network, selecting between coherent high-frequency oscillations, coherent gamma-band oscillations, and an intermediate transition state characterized by reduced synchrony. Importantly, while excitatory and inhibitory populations share a common oscillatory frequency within each regime, inhibitory neurons consistently exhibit greater population-level synchrony, indicating a dominant role for interneuron dynamics in pacing the network rhythm.

An important methodological consideration concerns the quantification of synchrony across different dynamical regimes. In this study, we employed both pairwise correlation of binned spike trains and the SPIKE-distance as complementary measures. While these metrics capture different aspects of coordination—rate cofluctuations and spike-time alignment, respectively—they are both based on pairwise interactions and can be affected by sparse firing. In particular, in regimes such as the high-frequency oscillatory state, excitatory neurons fire at low rates, reducing the probability of coincident spikes or precise temporal alignment across neuron pairs. As a result, both correlation-based and spike-timing-based measures may underestimate synchrony at the level of individual neuron pairs, even when coherent dynamics are present at the population level. Complementary approaches based on population-level statistics, such as the Fano factor of population spike counts [66], may provide additional insight into collective variability and coordination without relying on pairwise interactions. These considerations highlight the importance of interpreting synchrony measures in the context of firing statistics, and suggest that combining multiple, complementary metrics provides a more reliable characterization of network coordination across regimes.

The use of a timing-based, binning-independent measure (SPIKE-distance) confirms that the reduction in synchrony observed in the transition regime is robust and not an artifact of the chosen metric. These results highlight the importance of combining rate-based and timing-based measures when characterizing collective dynamics in spiking networks, particularly across regimes with different firing statistics.

Analysis of population phase relationships further demonstrates that the HFO and gamma states are characterized by stable but distinct patterns of excitatory-inhibitory coordination, whereas these relations become unstable within the transition regime. This suggests that the observed oscillatory modes correspond to separate dynamical states defined by regime-specific population coordination, rather than representing a continuous modulation of a single underlying mechanism.

Taken together, our results provide a dynamical framework linking the physiological diversity of inhibitory synaptic timescales to the emergence of distinct oscillatory regimes in recurrent cortical networks. By showing that inhibitory kinetics not only tune oscillation frequency but also organize excitatory-inhibitory coordination patterns, this work highlights a potential mechanism by which local circuit properties regulate the functional timescales of population activity and the stability of rhythmic communication in the brain.

ACKNOWLEDGMENT

M.P. acknowledges support from the Slovenian Research and Innovation Agency (Grant No. P1-0403).

DATA AVAILABILITY

There are no publicly available research data or software supporting this article. Requests for further information or data should be sent to the authors.

[1] G. Buzsáki, *Rhythms of the Brain* (Oxford University Press, New York, 2006).

[2] G. Buzsáki, Hippocampal sharp wave–ripple: A cognitive biomarker for episodic memory and planning, Hippocampus **25**, 1073 (2015).

[3] G. Buzsáki and F. Lopes da Silva, High frequency oscillations in the intact brain, Prog. Neurobiol. **98**, 241 (2012).

[4] G. Buzsaki and A. Draguhn, Neuronal oscillations in cortical networks, Science **304**, 1926 (2004).

[5] X.-J. Wang, Neurophysiological and computational principles of cortical rhythms in cognition, Physiol. Rev. **90**, 1195 (2010).

[6] A. K Engel and P. Fries, Beta-band oscillations—Signalling the status quo? Current Opin. Neurobiol. **20**, 156 (2010).

[7] W. Braun and R.-M. Memmesheimer, High-frequency oscillations and sequence generation in two-population models of hippocampal region CA_1, PLoS Comput. Biol. **18**, e1009891 (2022).

[8] L. L. Colgin, T. Denninger, M. Fyhn, T. Hafting, T. Bonnevie, O. Jensen, M.-B. Moser, and E. I Moser, Frequency of gamma oscillations routes flow of information in the hippocampus, Nature (London) **462**, 353 (2009).

[9] C. A. Bosman, J.-M. Schoffelen, N. Brunet, R. Oostenveld, A. M. Bastos, T. Womelsdorf, B. Rubehn, T. Stieglitz, P. De Weerd, and P. Fries, Attentional stimulus selection through selective synchronization between monkey visual areas, Neuron **75**, 875 (2012).

[10] P. Fries, Rhythms for cognition: Communication through coherence, Neuron **88**, 220 (2015).

[11] P. Fries, A mechanism for cognitive dynamics: Neuronal communication through neuronal coherence, Trends Cognit. Sci. **9**, 474 (2005).

[12] T. Womelsdorf and P. Fries, Modulation of neuronal interactions through neuronal synchronization, Science **316**, 1609 (2007).

[13] A. Ylinen, A. Bragin, Z. Nádasdy, G. Jandó, I. Szabo, A. Sik, and G. Buzsaki, Sharp wave-associated high-frequency oscillation (200 Hz) in the intact hippocampus: Network and intracellular mechanisms, J. Neurosci. **15**, 30 (1995).

[14] J. Csicsvari, H. Hirase, A. Czurko, A. Mamiya, and G. Buzsáki, Fast network oscillations in the hippocampal CA_1 region of the behaving rat, J. Neurosci. **19**, 274 (1999).

[15] G. Curio, B.-M. Mackert, M. Burghoff, R. Koetitz, K. Abraham-Fuchs, and W. Härer, Localization of evoked neuromagnetic 600 Hz activity in the cerebral somatosensory system, Electroencephalogr. Clin. Neurophysiol. **91**, 483 (1994).

[16] F. Grenier, I. Timofeev, and M. Steriade, Neocortical very fast oscillations (ripples, 80–200 Hz) during seizures: Intracellular correlates, J. Neurophysiol. **89**, 841 (2003).

[17] J. Taxidis, S. Coombes, R. Mason, and M. R Owen, Modeling sharp wave-ripple complexes through a CA_3-CA_1 network model with chemical synapses, Hippocampus **22**, 995 (2012).

[18] R. G. Averkin, V. Szemenyei, S. Bordé, and G. Tamás, Identified cellular correlates of neocortical ripple and high-gamma oscillations during spindles of natural sleep, Neuron **92**, 916 (2016).

[19] B. Williams, A. Vedururu Srinivas, R. Baravalle, F. R. Fernandez, C. C. Canavier, and J. A. White, Fast spiking interneurons autonomously generate fast gamma oscillations in the medial entorhinal cortex with excitation strength tuning ING–PING transitions, eNeuro **13**, ENEURO.0452-25.2026 (2026).

[20] X.-J. Wang and G. Buzsáki, Gamma oscillation by synaptic inhibition in a hippocampal interneuronal network model, J. Neurosci. **16**, 6402 (1996).

[21] N. Brunel and X.-J. Wang, What determines the frequency of fast network oscillations with irregular neural discharges? I. Synaptic dynamics and excitation-inhibition balance, J. Neurophysiol. **90**, 415 (2003).

[22] M. A. Whittington, R. D. Traub, and N. Kopell, Inhibition-based rhythms: Experimental and mathematical observations on network dynamics, Int. J. Psychophysiol. **38**, 315 (2000).

[23] E. O. Mann and O. Paulsen, Role of GABAergic inhibition in hippocampal network oscillations, Trends Neurosci. **30**, 343 (2007).

[24] M. Bartos, I. Vida, and P. Jonas, Synaptic mechanisms of synchronized gamma oscillations in inhibitory interneuron networks, Nat. Rev. Neurosci. **8**, 45 (2007).

[25] N. Roohi and A. Valizadeh, Role of interaction delays in the synchronization of inhibitory networks, Neural Comput. **34**, 1425 (2022).

[26] P. Tiesinga and T. J. Sejnowski, Cortical enlightenment: Are attentional gamma oscillations driven by ING or PING? Neuron **63**, 727 (2009).

[27] J. A. Cardin, M. Carlén, K. Meletis, U. Knoblich, F. Zhang, K. Deisseroth, L.-H. Tsai, and C. I. Moore, Driving fast-spiking cells induces gamma rhythm and controls sensory responses, Nature (London) **459**, 663 (2009).

[28] A. Hasenstaub, Y. Shu, B. Haider, U. Kraushaar, A. Duque, and D. A McCormick, Inhibitory postsynaptic potentials carry synchronized frequency information in active cortical networks, Neuron **47**, 423 (2005).

[29] V. S. Sohal, F. Zhang, O. Yizhar, and K. Deisseroth, Parvalbumin neurons and gamma rhythms enhance cortical circuit performance, Nature (London) **459**, 698 (2009).

[30] M. Khanjanianpak, N. Azimi-Tafreshi, and A. Valizadeh, Emergence of complex oscillatory dynamics in the neuronal networks with long activity time of inhibitory synapses, iScience **27**, 109401 (2024).

[31] P. Jonas, J. Bischofberger, D. Fricker, and R. Miles, Interneuron diversity series: Fast in, fast out—Temporal and spatial signal processing in hippocampal interneurons, Trends Neurosci. **27**, 30 (2004).

[32] M. Farrant and Z. Nusser, Variations on an inhibitory theme: Phasic and tonic activation of $GABA_a$ receptors, Nat. Rev. Neurosci. **6**, 215 (2005).

[33] S. Hefft and P. Jonas, Asynchronous GABA release generates long-lasting inhibition at a hippocampal interneuron–principal neuron synapse, Nat. Neurosci. **8**, 1319 (2005).

[34] M. Bartos, I. Vida, M. Frotscher, J. R. P. Geiger, and P. Jonas, Rapid signaling at inhibitory synapses in a dentate gyrus interneuron network, J. Neurosci. **21**, 2687 (2001).

[35] M. Bartos, I. Vida, M. Frotscher, A. Meyer, H. Monyer, J. R. P. Geiger, and P. Jonas, Fast synaptic inhibition promotes synchronized gamma oscillations in hippocampal interneuron networks, Proc. Natl. Acad. Sci. USA **99**, 13222 (2002).

[36] R. Tremblay, S. Lee, and B. Rudy, GABAergic interneurons in the neocortex: From cellular properties to circuits, Neuron **91**, 260 (2016).

[37] C. Geisler, N. Brunel, and X.-J. Wang, Contributions of intrinsic membrane dynamics to fast network oscillations with irregular neuronal discharges, J. Neurophysiol. **94**, 4344 (2005).

[38] N. Brunel, Dynamics of sparsely connected networks of excitatory and inhibitory spiking neurons, J. Comput. Neurosci. **8**, 183 (2000).

[39] Q. Wang, M. Perc, Z. Duan, and G. Chen, Synchronization transitions on scale-free neuronal networks due to finite information transmission delays, Phys. Rev. E **80**, 026206 (2009).

[40] C. Börgers and N. Kopell, Synchronization in networks of excitatory and inhibitory neurons with sparse, random connectivity, Neural Comput. **15**, 509 (2003).

[41] Q. Wang, G. Chen, and M. Perc, Synchronous bursts on scale-free neuronal networks with attractive and repulsive coupling, PLoS One **6**, e15851 (2011).

[42] V. Volman, M. Perc, and M. Bazhenov, Gap junctions and epileptic seizures—two sides of the same coin? PLoS One **6**, e20572 (2011).

[43] D. Fan, Q. Wang, and M. Perc, Disinhibition-induced transitions between absence and tonic-clonic epileptic seizures, Sci. Rep. **5**, 12618 (2015).

[44] H. C. Tuckwell, *Introduction to Theoretical Neurobiology: Linear Cable Theory and Dendritic Structure* (Cambridge University Press, Cambridge, UK, 1988), Vol. 1.

[45] W. Gerstner and W. M Kistler, *Spiking Neuron Models: Single Neurons, Populations, Plasticity* (Cambridge university press, Cambridge, UK, 2002).

[46] P. Dayan and L. F Abbott, *Theoretical Neuroscience: Computational and Mathematical Modeling of Neural Systems* (MIT Press, Cambridge, MA, USA, 2005).

[47] T. P. Vogels and L. F. Abbott, Signal propagation and logic gating in networks of integrate-and-fire neurons, J. Neurosci. **25**, 10786 (2005).

[48] A. Destexhe, Z. Mainen, and T. J. Sejnowski, An effcient method for computing synaptic conductances based on a kinetic model of receptor binding, Neural Comput. **6**, 14 (1994).

[49] M.-O. Gewaltig and M. Diesmann, Nest (neural simulation tool), Scholarpedia, **2**, 1430 (2007).

[50] J. M. Eppler, M. Helias, E. Muller, M. Diesmann, and M.-O. Gewaltig, PyNEST: A convenient interface to the NEST simulator, Front. Neuroinf. **2**, 363 (2009).

[51] C. R. Harris *et al.*, Array programming with NumPy, Nature (London) **585**, 357 (2020).

[52] P. Virtanen *et al.*, SciPy 1.0: Fundamental algorithms for scientific computing in Python, Nat. Methods **17**, 261 (2020).

[53] W. McKinney *et al.*, Data structures for statistical computing in Python, in *Proceedings of the 9th Python in Science Conference* (SciPy, 2010), pp. 56–61.

[54] J. D Hunter, Matplotlib: A 2D graphics environment, Comput. Sci. Eng. **9**, 90 (2007).

[55] S. Kheiri, Inhibitory timescale transitions regime [source code], GitHub repository (2026), https://github.com/siamakkheiri/inhibitory-timescale-transitions-regime.

[56] A. Renart, J. De La Rocha, P. Bartho, L. Hollender, N. Parga, A. Reyes, and K. D. Harris, The asynchronous state in cortical circuits, Science **327**, 587 (2010).

[57] T. Kreuz, D. Chicharro, M. Greschner, and R. G Andrzejak, Time-resolved and time-scale adaptive measures of spike train synchrony, J. Neurosci. Methods **195**, 92 (2011).

[58] T. Kreuz, D. Chicharro, C. Houghton, R. G Andrzejak, and F. Mormann, Monitoring spike train synchrony, J. Neurophysiol. **109**, 1457 (2013).

[59] E. Satuvuori, M. Mulansky, N. Bozanic, I. Malvestio, F. Zeldenrust, K. Lenk, and T. Kreuz, Measures of spike train synchrony for for data with multiple time scales, J. Neurosci. Methods **287**, 25 (2017).

[60] M. Mulansky and T. Kreuz, PySpike—A Python library for analyzing spike train synchrony, SoftwareX **5**, 183 (2016).

[61] G. Curio, B. M. Mackert, M. Burghoff, R. Koetitz, K. Abraham-Fuchs, and L. Harms, High-frequency (200 Hz) ripples in the human neocortex, Neurosci. Lett. **179**, 139 (1994).

[62] A. Pariz, Z. G Esfahani, S. S Parsi, A. Valizadeh, S. Canals, and C. R Mirasso, High frequency neurons determine effective connectivity in neuronal networks, NeuroImage **166**, 349 (2018).

[63] A. Pariz, I. Fischer, A. Valizadeh, and C. Mirasso, transmission delays and frequency detuning can regulate information flow between brain regions, PLoS Comput. Biol. **17**, e1008129 (2021).

[64] A. Ziaeemehr, M. Zarei, A. Valizadeh, and C. R. Mirasso, Frequency-dependent organization of the brain's functional network through delayed-interactions, Neural Networks **132**, 155 (2020).

[65] E. Bolhasani, Y. Azizi, A. Valizadeh, and M. Perc, Synchronization of oscillators through time-shifted common inputs, Phys. Rev. E **95**, 032207 (2017).

[66] H. Rezaei, A. Aertsen, A. Kumar, and A. Valizadeh, Facilitating the propagation of spiking activity in feedforward networks by including feedback, PLoS Comput. Biol. **16**, e1008033 (2020).